Journal of Remote Sensing
A SCIENCE PARTNER JOURNAL

RESEARCH ARTICLE

An Operational Assessment Framework for Near Real-time Cropland Dynamics: Toward Sustainable Cropland Use in Mid-Spine Belt of Beautiful China

Zhenrong Du[1], Le Yu[1,2,3*], Xin Chen[1], Xiyu Li[1], Dailiang Peng[4,5], Shijun Zheng[4,5,6], Pengyu Hao[7], Jianyu Yang[8], Huadong Guo[4], and Peng Gong[2,9]

[1]Department of Earth System Science, Ministry of Education Key Laboratory for Earth System Modeling, Institute for Global Change Studies, Tsinghua University, Beijing 100084, China. [2]Ministry of Education Ecological Field Station for East Asian Migratory Birds, Beijing 100084, China. [3]Tsinghua University (Department of Earth System Science)-Xi'an Institute of Surveying and Mapping Joint Research Center for Next-Generation Smart Mapping, Beijing 100084, China. [4]Key Laboratory of Digital Earth Science, Aerospace Information Research Institute, Chinese Academy of Sciences, Beijing 100094, China. [5]International Research Center of Big Data for Sustainable Development Goals, Beijing 100094, China. [6]University of Chinese Academy of Sciences, Beijing 100049, China. [7]Food and Agriculture Organization of the United Nations, Viale delle Terme di Caracalla, 00153 Rome, Italy. [8]College of Land Science and Technology, China Agricultural University, Beijing 100193, China. [9]Department of Geography, Department of Earth Sciences and Institute for Climate and Carbon Neutrality, University of Hong Kong, Hong Kong 999077, China.

*Address correspondence to: leyu@tsinghua.edu.cn

Citation: Du Z, Yu L, Chen X, Li X, Peng D, Zheng S, Hao P, Yang J, Guo H, Gong P. An Operational Assessment Framework for Near Real-time Cropland Dynamics: Toward Sustainable Cropland Use in Mid-Spine Belt of Beautiful China. *J. Remote Sens.* 2023;3:Article 0065. https://doi.org/10.34133/remotesensing.0065

Submitted 6 December 2022
Accepted 9 July 2023
Published 27 July 2023

Cropland monitoring is a crucial component for a broad user community from Land Use and Land Cover Change study to food security policy making. Faced with the rich natural ecological environment and variable agricultural production conditions of Mid-Spine Belt of Beautiful China (MSBBC), this study developed a novel operational assessment framework that combined the near real-time land cover mapping platform (i.e., FROM-GLC Plus), the FAO Agricultural Stress Index System, and the land degradation monitoring method suggested by United Nations Convention to Combat Desertification for the timely monitoring of cropland extent change, cropland conditions, and cropland degradation. With integrated monitoring system, this framework can provide convenient access to high-spatiotemporal-resolution cropland maps (30 m, dekadal) and instant (near real time) cropland dynamics. According to the monitoring results, we found that the abnormally high temperatures of summer 2022 adversely affected crop health in the southwest of MSBBC. Besides, our results suggested that China's ecological restoration projects made remarkable achievement in MSBBC. The productivity of more than 70% of cropland in MSBBC has improved, and only ~6% cropland (~3.69×10^4 km^2) has degraded since 2000, mainly distributed in cropland with steep slope, insufficient precipitation, and intensive use. Site-specific measures, such as conservation tillage, improved tillage systems, and cropland ecological projects, should be adopted for sustainable cropland use and further increase in land carrying capacity of MSBBC to achieve balanced east-west development in China.

Introduction

Over the last decades, the global increasing population has added the pressure on food supplies and cropland resources [1–3]. As cropland declines and degrades, especially in ecologically fragile areas such as farming-pastoral ecotone, this pressure is further exacerbated [4–7]. Besides, frequent climatic anomalies in recent years, such as high temperatures, require a near real-time grasp of cropland conditions for timely interventions and policy adjustments [8–10]. Therefore, precise and timely monitoring of cropland dynamics is crucial for world's food security research, water management, agricultural planning, and sustainable development [11–16].

Based on its geographical background of China's crop-pasture band, the Mid-Spine Belt of Beautiful China (MSBBC) serves as an important agricultural space and ecological security

barrier, which blocks the continuation of desertification to the south and protects a large area of cropland in the major agricultural areas of eastern China [17–19]. Due to water overexploitation and agriculture–animal husbandry imbalance, resources and environmental pressures have been increasing in MSBBC for a long time [20,21]. Ecological and environmental problems such as land desertification and soil erosion caused by natural and man-made factors have led to a decline in soil fertility and food production, a high incidence of cropland abandonment, and an increase in the conflict between people and land [7,22]. Therefore, obtaining reliable and timely cropland monitoring data of MSBBC is important for sustainable cropland use, synergistic development of agriculture and pastoralism, and achieving balanced east-west development in China.

Thanks to the immediacy and objectivity of remote sensing technology, as well as the public access to Landsat imagery, cropland dynamic monitoring results can now be obtained economically and efficiently on a large scale, giving rise to the emergence of cropland monitoring projects, such as Crop Explorer, CropWatch, Global Agriculture Monitoring, Monitoring Agricultural Resources, Famine Early Warning Systems Network, and Global Information and Early Warning System [23–29]. These projects are critical to offering timely and reliable information on cropland distribution, cropland conditions. Taking advantage of multisource remote sensing datasets and solid field works, these projects demonstrate strong strengths in continuous monitoring and production forecasting, which contributes to the agricultural monitoring and food security ensuring [30,31]. However, the disadvantages of these projects are also noteworthy. The currently available cropland products absence of precise spatial location of the cropped areas due to the hysteresis and the coarse resolution nature of the map products with substantial uncertainties in areas, locations, and detail [32,33]. In addition, the monitoring of cropland conditions is developed based on the vegetation indexes and weather dynamics collected from remote sensing images, lacking the consideration of integrated indicators such as drought intensity and agricultural stress. Furthermore, monitoring of cropland degradation is not included in these projects, let alone near real-time monitoring for the purpose of early warning.

Precise and timely cropland maps are the basis of the cropland monitoring. Although remote sensing data used for Earth observation are now available quickly and easily, near real-time high-spatial- and temporal-resolution land cover mapping is still challenging because of the uneven spatiotemporal distribution of data and time-consuming training sample collection [34,35]. In parallel with Sentinel 2 images, Google Dynamic World developed an automated framework to provide land cover predictions in near real time [36]. The single-date classification fashion of Google Dynamic World allows the extremely up-to-date land cover map globally but also leads to spatiotemporal discontinuities in the classification results. Besides, due to the use of Sentinel 2 imagery, this land cover dataset is not available prior to 2015. Based on Finer Resolution Observation and Monitoring–Global Land Cover (FROM-GLC) [37] and Google Earth Engine (GEE) [38], FROM-GLC Plus is another automated framework developed for near real-time land cover mapping [34]. Using multiseason sample migration, multisource data time series reconstruction, and machine learning, FROM-GLC Plus can produce historically comparable and near real-time land cover maps, enabling the cropland dynamics monitoring in this paper.

Cropland condition monitoring is a vital function of agricultural monitoring projects. As mentioned before, the indicators typically used are vegetation indexes and weather dynamics derived from remote sensing imagery (e.g., CropExplorer and Global Agriculture Monitoring). To provide alternative measures of crop health and growing conditions, the Food and Agriculture Organization of the United Nations (FAO) developed the Agricultural Stress Index System (ASIS) using composite indexes obtained from traditional vegetation index of NDVI and temperature over the crop growing season [39]. These indexes can offer a more comprehensive perspective for the drought degrees and agricultural stress with a 10-d (dekadal) update frequency and are thus included in the monitoring framework developed in this paper.

Another important but long neglected indicator is the monitoring of cropland degradation. For ecologically fragile areas, such as crop–pasture band and semiarid areas, cropland degradation is a common consequence of topography, climate and land use policies [40,41]. Faced with land degradation, one of the most serious global environmental problems, the United Nations General Assembly adopted the "Transforming Our World: The 2030 Agenda for Sustainable Development" in September 2015, clearly stating that achieving a world with zero land degradation is one of the important goals of the Sustainable Development Goals (SDGs) [42]. To achieve this goal, the United Nations Convention to Combat Desertification (UNCCD) proposed and improved a set of implementable land degradation monitoring methods in 2017 and 2021, respectively. These methods are specifically designed to quantify the SDG indicator 15.3.1 (Proportion of land that is degraded over total land area). This indicator was elevated to Tier 1 in 2019, allowing it to be quantified using the UNCCD monitoring methods on a global scale. Recently, the methods have been successfully applied to arid and semiarid regions, such as Inner Mongolia, China [43], Tanzania [44], and globally [45], providing valuable insights and estimation bases for near real-time monitoring of cropland degradation within our operational assessment framework [46,47].

In this paper, we developed a novel and comprehensive operational assessment framework for cropland dynamic monitoring in MSBBC that integrates multiple technologies, including the near real-time land cover mapping platform FROM-GLC Plus, the FAO ASIS, and the land degradation monitoring method suggested by UNCCD. By synergistically utilizing these methods, we are able to achieve a higher spatiotemporal resolution and timeliness in monitoring cropland extent change, cropland conditions, and cropland degradation while also enhancing the overall comprehensiveness of cropland monitoring indicators. This framework represents a step forward in improving the ability to monitor and manage cropland resources in a more sustainable manner. Additionally, we analyzed the current cropland change and degradation and further discussed potential measures for sustainable cropland use in the MSBBC.

Materials and Methods

Study area

The study area of MSBBC is proposed to analyze the possible future change of Hu Line and promote the balanced development of the east and west of China (Fig. 1). The Hu Line is a boundary marking Chinese population density differences which was proposed in

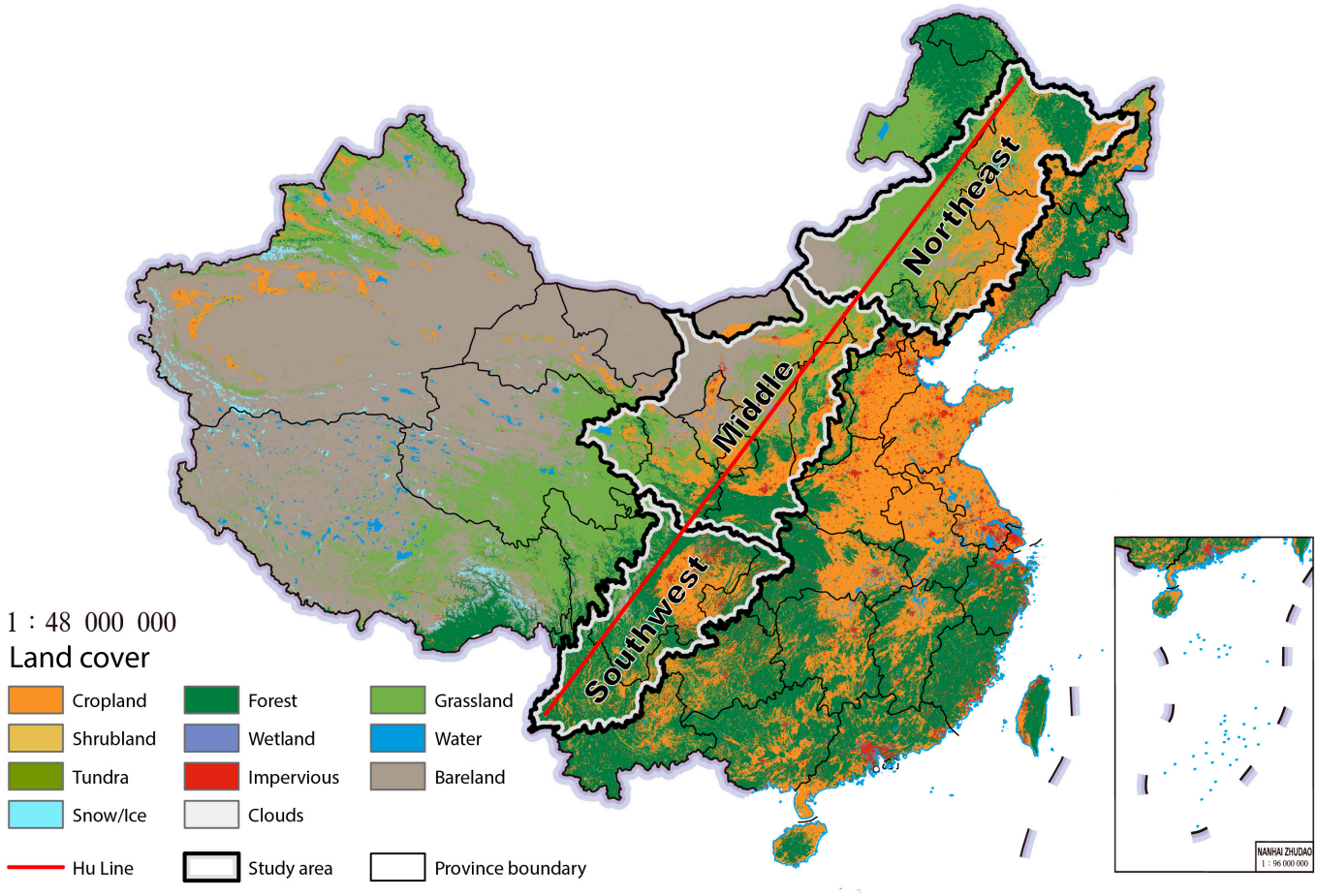

Fig. 1. The study area of MSBBC. (The 2021 land cover map of China is from FROM-GLC Plus [34].)

1935 based on the county-level populations [48]. This line ran from Aihui, Heilongjiang Province to Tengchong, Yunnan Province, reflecting the spatial differences in natural environment and socio-economic development in China [19]. MSBBC is divided into a northeast section, a middle section, and a southwest section, based on aspects of nature, society, economy, and culture.

MSBBC covers an area of about 240 km^2, which is about a quarter of China's land area. It spans different natural zones and has a rich diversity of natural ecosystems, including boreal and temperate high montane forests and woodland, temperate subhumid grasslands, semidesert steppes, etc., according to the International Union for Conservation of Nature Global Ecosystem Typology [49]. The topography of the region varies dramatically, with an overall trend of gradually increasing elevation from the northeast to the southwest, crossing the Northeast Plain, Inner Mongolia Plateau, Loess Plateau, Sichuan Basin, Qinghai-Tibet Plateau, and Yunnan-Guizhou Plateau. Since most of the MSBBC is located in the farming-pastoral ecotone of China, its agricultural structure shows a mixture of animal husbandry and plantation. However, the deteriorating ecological environment and sloppy management practices have led to the abandonment, sanding, and degradation of a large amount of cropland in MSBBC [50–52], making it imperative to understand the cropland dynamics for sustainable agriculture.

Data

In order to develop the assessment framework for near real-time cropland dynamics, a wide range of data sources were integrated, including multisource satellite imagery, key indicators sourced from the Food and Agriculture Organization of the United Nations Agricultural Stress Index System (FAO ASIS), as well as other auxiliary datasets (Table 1). To overcome the challenge of data scale mismatch arising from varying spatial resolutions of the datasets, all the imagery used in the analysis was subject to resizing and reprojection, with a bicubic interpolation algorithm used to ensure consistent spatial resolution at 30 m.

Satellite imagery

Satellite imagery from Landsat and Moderate Resolution Imaging Spectroradiometer (MODIS) was used for land cover classification, cropland conditions, and degradation monitoring in this study. For Landsat imagery, this study used Landsat Tier 1 surface reflectance images available in GEE, including imagery from the Landsat Thematic Mapper (TM), Enhanced Thematic Mapper Plus (ETM+), and Operational Land Imager (OLI) sensors of 2000, 2015, and 2022. As for MODIS imagery, the 500-m MODIS MCD43A4 Version 6 NBAR product is used for land cover mapping to fill in Landsat time series gaps. The 500-m MODIS products, including MOD17A2H Terra Gross Primary Productivity (GPP) and MOD13A1 Terra Vegetation Indices, are used for cropland condition monitoring and degradation monitoring.

Indicators in FAO ASIS

The ASIS is an agricultural monitoring system developed by the FAO, using Advanced Very High Resolution Radiometer

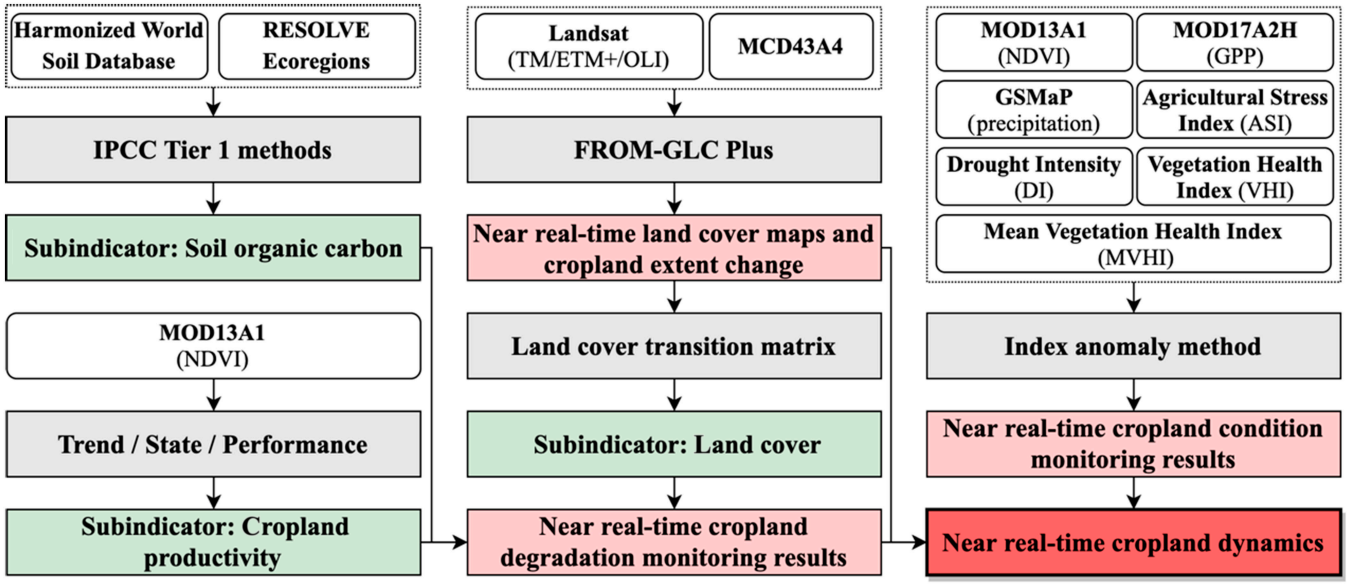

Fig. 2. Workflow for near real-time cropland dynamics monitoring.

imagery at 1-km resolution. The FAO ASIS provides near real-time global agricultural monitoring datasets updated every 10 d, including Agricultural Stress Index (ASI), Drought Intensity (DI), Mean Vegetation Health Index (MVHI), Vegetation Condition Index, and Vegetation Health Index (VHI). The ASIS datasets can be publicly accessed by Web Map Service and GEE.

Auxiliary data

In addition to FAO ASIS datasets and satellite imagery from Landsat and MODIS, the cropland condition and degradation monitoring in this study also rely on some ancillary datasets including Global Satellite Mapping of Precipitation (GSMaP) product [53], the Harmonized World Soil Database (HWSD) [54], RESOLVE Ecoregions dataset [55].

Based on the global land cover change near real-time monitoring platform (i.e., FROM-GLC Plus) [34], FAO ASIS [39], and the land degradation monitoring method suggested by UNCCD [46,47], this study intends to carry out 10-d updated near real-time monitoring of cropland extent change and crop conditions and to conduct near real-time monitoring of cropland degradation based on 3 aspects: land cover, cropland productivity, and soil organic carbon (Fig. 2).

Near real-time land cover mapping and cropland extent change monitoring with FROM-GLC Plus

Near real-time land cover maps can be used to provide immediate distribution of cropland extent in the study area. Meanwhile, combined with the historical land cover mapping results, current cropland degradation can be further analyzed and quantified. In this study, historical and near real-time land cover maps were developed with FROM-GLC Plus [34]. Taking advantage of multisource data fusion, multiseason sample migration and machine learning, FROM-GLC Plus is developed with the aim to provide a framework for capturing land cover maps in near real-time at multitemporal (annual to daily) and multiresolution (30 m to submeter) levels. Considering the sparsity of valid Landsat time series, MCD43A4 images were used to reconstruct the spectral time series with spatiotemporal fusion methods developed by FROM-GLC Plus. For the land cover mapping in this study, 11 spectral bands of March to October were used, including Blue, Green, Red, Near Infrared (NIR), Shortwave Infrared 1 (SWIR1), Shortwave Infrared 2 (SWIR2), NDVI, EVI, Normalized Burn Ratio (NBR), Normalized Difference Built-up Index (NDBI), and Modified Normalized Difference

Table 1. The usage and details of multisource datasets used in this study.

No.	Name	Spatial resolution	Temporal resolution	Usage in this study
1.	Landsat TM/ETM+/OLI	30 m	16 d	Land cover mapping
2.	MCD43A4	500 m	Daily	
3.	MOD17A2H	500 m	8 d	Cropland condition monitoring
4.	FAO ASIS	1 km	10 d	
5.	GSMaP	0.1 degree	Hourly	
6.	MOD13A1	500 m	16 d	Cropland condition and degradation monitoring
7.	HWSD	30 arc-second	-	Cropland degradation monitoring
8.	RESOLVE Ecoregions	Vector dataset	-	

FAO ASIS, Food and Agriculture Organization of the United Nations Agricultural Stress Index System; GSMaP, Global Satellite Mapping of Precipitation; HWSD, Harmonized World Soil Database.

Water Index (MNDWI). The feature space for land cover mapping was then developed using the per-pixel maximum, mean, standard deviation, and 10, 20, 30, 40, 50, 60, 70, 80, 90 percentiles of each band. Furthermore, sample migration is realize using feature space similarity and difference measures based on the first all-season sample set (FAST) collected in 2015 [34]. Finally, land cover maps of 2000, 2015, and near real time (2022 August 20 and can be updated dekadally) in the study area with 30-m resolution can be obtained using Random Forest.

Near real-time cropland condition monitoring with MODIS and FAO ASIS

In order to realize fast and near real-time monitoring, the cropland condition monitoring in this study is developed based on index anomaly method. Specifically, the monitoring indexes are shown in Table 2, including GPP, Normalized Difference Vegetation Index (NDVI), Precipitation (PR), ASI, DI, MVHI, and VHI. Cropland conditions can be rapidly and automatically assessed by comparing monitoring indexes of current and previous years. For a given monitoring period, assume that $Index_{avg}$ and $Index_{std}$ are the average and standard deviation of the monitoring index over the previous 5 years, $Index_{target}$ is the monitoring index value of the target period. Taking GPP as an example, if $Index_{target} > Index_{avg} + Index_{std}$, the condition is defined as "Better"; if $Index_{target} < Index_{avg} - Index_{std}$, the condition is defined as "Worse"; if $Index_{target} \geq Index_{avg} - Index_{std}$ and $Index_{target} \leq Index_{avg} + Index_{std}$, the condition is defined as "Similar". By providing the monitoring results obtained from each monitoring index, the growing environment (such as PR) and crop conditions (such as VHI) can be obtained.

Near real-time cropland degradation monitoring

Based on the near real-time land cover maps and cropland conditions monitoring results, the cropland degradation monitoring followed the framework proposed by UNCCD [46,47]. The assessment of cropland degradation was conducted separately with 3 subindicators of land cover, land productivity, and soil organic carbon, and the results are integrated to obtain the final monitoring result using a one-out-all-out (1OAO) method with 10-d update frequency, in which land degradation is determined when any of the 3 subindicators shows degradation (Fig. 3).

Subindicator: Land cover

For the land cover subindicator, cropland degradation monitoring was mainly implemented based on the land cover transition matrix. The dekadally updated land cover maps used for this subindicator were obtained using FROM-GLC Plus introduced in "Near real-time land cover mapping and cropland extent change monitoring with FROM-GLC Plus". Firstly, the classification system of FROM-GLC should be harmonized to Intergovernmental Panel on Climate Change (IPCC) classes (Table 3). Secondly, the land cover transition matrix is generated according to the UNCCD framework and ecological engineering (i.e., returning cropland to forest/grassland) in the study area (Table 4). Thirdly, the cropland degradation extent of baseline period (2000 to 2015) and target period (2015 to near real time) was obtained using the transition matrix. Finally, the cropland degradation assessment result of the target period was developed based on the cropland degradation extent of the 2 periods. Specifically, if "degradation" or "improvement" in the target period, then it would be considered as "degradation" or "improvement"; if "stable" in the target period, "degradation", "improvement" or "stable" would be determined by the status in the baseline period.

Subindicator: Cropland productivity

The cropland productivity degradation was performed from 3 aspects: *Trend*, *State*, and *Performance*. The index used to indicate the productivity of cropland in this study was NDVI which can be obtained from the 500-m and 16-d updated MOD13A1 imagery during 2000 to 2022. Specifically, the NDVI time series were constructed using the mean value of NDVI of annual growing seasons (March to October) for subsequent calculation.

Trend is measured using the trajectory of productivity change over the long term for both baseline and target period. The cropland productivity trend was evaluated using ridge regression on GEE. If $p < 0.01$ and $slope > 0$, the pixel would be measured as "improvement"; If $p < 0.01$ and $slope < 0$, the

Table 2. The data source of cropland condition monitoring indexes.

No.	Index		Data source		
	Name	Temporal resolution	Name	Spatial resolution	Temporal resolution
1.	Gross Primary Productivity (GPP)	8 d	MOD17A2H	500 m	8 d
2.	Normalized Difference Vegetation Index (NDVI)	16 d	MOD13A1	500 m	16 d
3.	Precipitation (PR)	10 d	GSMaP	0.1 degree	Hourly
4.	Agricultural Stress Index (ASI)	10 d	FAO ASIS	1 km	10 d
5.	Drought Intensity (DI)	10 d	FAO ASIS	1 km	10 d
6.	Mean Vegetation Health Index (MVHI)	10 d	FAO ASIS	1 km	10 d
7.	Vegetation Health Index (VHI)	10 d	FAO ASIS	1 km	10 d

GSMaP, Global Satellite Mapping of Precipitation; FAO ASIS, Food and Agriculture Organization of the United Nations Agricultural Stress Index System.

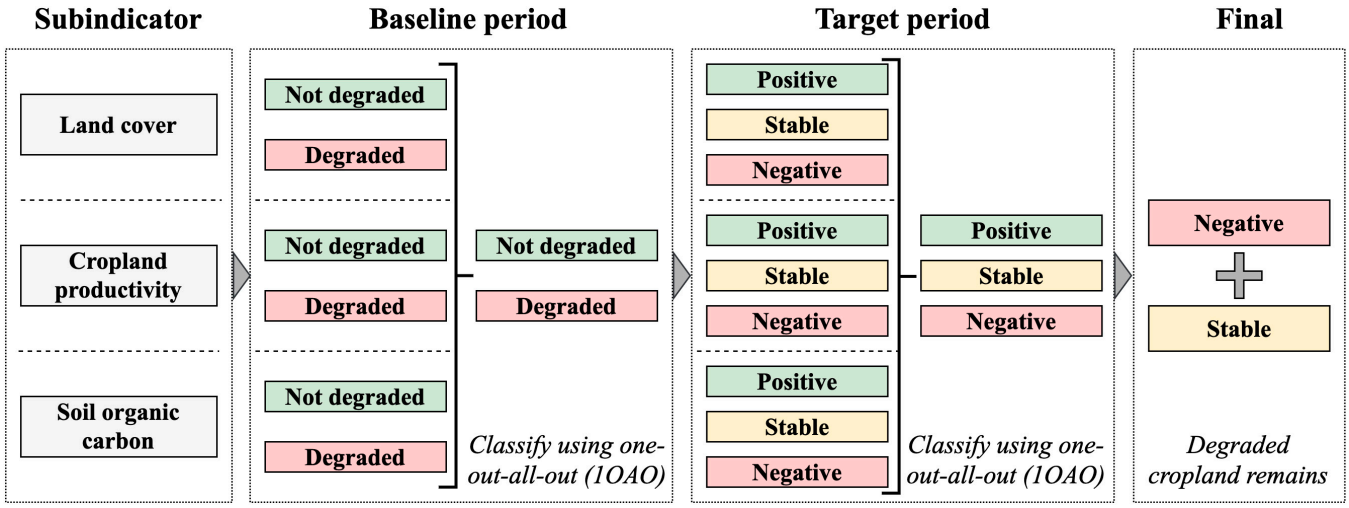

Fig. 3. UNCCD workflow to obtain final degraded cropland from subindicators of land cover, cropland productivity, and soil organic carbon [46,47].

pixel would be measured as "degradation"; otherwise, the pixel would be measured as "stable".

State is calculated by comparing the mean annual NDVI of the baseline and target periods. Firstly, the mean (μ) and standard deviation (σ) of annual NDVI during the baseline period were calculated. Then, the mean of annual NDVI during the target period was obtained as $\bar{x}$, and the significance was calculated as follows:

$$Z = \frac{\bar{x} - \mu}{\sigma / \sqrt{3}} \quad (1)$$

If $Z < -1.96$, the pixel was determined as "degradation"; if $Z > 1.96$, the pixel was determined as "improvement"; otherwise, the pixel was determined as "stable".

Performance is used to indicate spatial differences in cropland productivity within regions. In this study, the division of regions is based on the dataset of RESOLVE Ecoregions [55]. For each region, *Performance* was calculated by comparing it to the maximum NDVI value observed. The 90th percentile of NDVI within the region was used as $NDVI_{max}$ to avoid overestimation of the maximum value due to outliers. For each pixel, *Performance* was calculated as follows:

$$Performance = \frac{NDVI_{observed}}{NDVI_{max}} \quad (2)$$

An output *Performance* value close to 1 indicates that the pixel has the highest productivity level for the period. As suggested by UNCCD, pixels with *Performance* < 0.5 were marked as degraded.

Finally, the pixel-level cropland productivity degradation was assessed by the combination of *Trend*, *State*, and *Performance* based on the lookup table shown in Table 5.

Subindicator: Soil organic carbon

In this study, the pixel-level change of soil organic carbon stocks was estimated based on the dekadally updated land cover maps using IPCC Tier 1 methods [56] as follows:

$$SOC = SOC_{Ref} \times F_{LU} \times F_{MG} \times F_I \quad (3)$$

where SOC represents the soil organic carbon stocks; SOC_{Ref} is the common set of reference soil organic carbon stocks; F_{LU}, F_{MG}, F_I are default stock change factors determined by temperature and soil moisture regimes, which are provided by IPCC [56], and represent stock change factor for land-use systems/subsystem for a particular land-use, management regime, input of organic matter, respectively.

Once SOC was obtained for the baseline and target periods, the relative percentage change was calculated as $r_{SOC} = \frac{SOC_{baseline} - SOC_{target}}{SOC_{baseline}} \times 100\,\%$. If $r_{SOC} < -10\%$, the pixel was marked as "degradation"; if $r_{SOC} > 10\%$, the pixel was marked as "improvement"; otherwise, the pixel was marked as "stable".

Table 3. Mapping between FROM-GLC classification system and IPCC classes.

IPCC classes	FROM-GLC classes
Cropland	Cropland
Forest land	Forest
Grassland	Grassland
	Shrubland
Wetlands	Wetland
Settlements	Impervious
Other land	Tundra
	Water
	Bare land
	Ice/snow

Results and Discussion

Spatiotemporal dynamics of cropland in MSBBC from 2000 to near real time

Taking advantage of the FROM-GLC Plus, land cover maps of 2000, 2015, and near real time (2022 August 20) of MSBBC

Table 4. Land cover transition matrix using IPCC classes [46,47].

Current Previous	Forest land	Grassland	Cropland	Wetlands	Settlements	Other land
Forest land	Stable	Degradation	Degradation	Degradation	Degradation	Degradation
Grassland	Improvement	Stable	Degradation	Improvement	Degradation	Degradation
Cropland	Improvement	Improvement	Stable	Improvement	Degradation	Degradation
Wetlands	Degradation	Degradation	Degradation	Stable	Degradation	Degradation
Settlements	Improvement	Improvement	Improvement	Improvement	Stable	Improvement
Other land	Improvement	Improvement	Improvement	Improvement	Degradation	Stable

were developed and shown in Fig. 4A to C, respectively. To evaluate the accuracy of the land cover maps, evaluation samples were generated using the FROM-GLC Plus, and the overall accuracy for the years 2000, 2015, and near real-time maps are 0.76, 0.73, and 0.72, respectively, indicating a high level of accuracy and consistency across different time periods. Cropland and natural vegetation (forest, shrubland, and grassland) are mainly located to the east of the Hu Line, whereas the land cover in the west of the Hu Line is dominated by bare land and grassland. Large tracts of cropland are concentrated in the open area of the Northeast Plain, the Loess Plateau and the Sichuan Basin. In addition, the cropland dynamics during 2000 and near real time can be obtained in the annual land cover maps and cropland transfer analysis in Fig. 4D. Generally, over the last 2 decades, the amount of cropland lost has been greater than the amount gained. Urban expansion is an important reason for the occupation of cropland, as a large proportion of it is converted to impervious cover. Besides, China's revegetation programs have resulted in the conversion of large amounts of cropland to forest, grassland, and shrubland. According to our result, the area of cropland converted as a result of China's revegetation programs is about twice as large as the area converted to bare land, which demonstrates the effectiveness of ecological restoration projects launched in China. Meanwhile, newly cleared cropland is also found, mostly occupying grassland and bare land, which is typical in agro-pastoral ecotone.

Table 5. Lookup table for determining cropland productivity degradation [46,47].

No.	Trend	State	Performance	Combination
1.	Y	Y	Y	Y
2.	Y	Y	N	Y
3.	Y	N	Y	Y
4.	Y	N	N	Y
5.	N	Y	Y	Y
6.	N	Y	N	N
7.	N	N	Y	N
8.	N	N	N	N

Y is degraded/improved and N is not degraded/improved.

Furthermore, detailed annual cropland expansion and contraction were shown in Fig. 5, including (a) cropland expansion on the Songnen Plain, northeast China; (b) cropland contraction caused by urban sprawl on Loess Plateau, northwest China. Google Earth images illustrate how land change dynamics.

Near real-time cropland condition in MSBBC

Using indexes shown in Table 1, the near real-time (2022 August 20) cropland condition monitoring in this study is developed based on the cropland extent using index anomaly method (Fig. 6). According to the PR monitoring results, most regions of the study area have less precipitation than previous years, which further results in the distribution of large areas of higher DI. However, in accordance with the monitoring results of VHI, which is an index calculated using NDVI and temperature, drought does not directly cause a decline in the crop health. For the northeast and middle section of MSBBC, the crop health shows similar or even better than previous years. The decline in crop health is mainly seen in the Sichuan basin and mountainous areas located in the southwest, which may be related to the unusually and persistent high temperatures in these regions in the summer of 2022. As a complement, this can also be observed in the monitoring results of NDVI. Furthermore, if we include the VHI for the entire 2022 growing season (until August) in the monitoring, which is represented by MVHI, most areas do not show a substantial decline in crop health. If the hot and arid weather ends in time or if timely human interventions (such as irrigation or shade) are provided, crop growth may still return to previous years' levels. Also, ASI is an indicator calculated from the VHI throughout the growing season, but it is obtained after taking into account the sensitivity of the crop to water stress. Based on the monitoring results of ASI, higher agricultural stress can be observed on the sides of Hu Line as well as in the higher elevations of the mountainous areas with fragmented cropland and complicated environment. Besides, the GPP monitoring results also reflect this from a productivity perspective. Topographical and soil conditions, lack of irrigation measures, difficulties in access to water sources, and sloppy management practices may all contribute to this phenomenon, especially in the context of the unusually high temperature of 2022 in China.

Near real-time cropland degradation in MSBBC

Taking advantages of the near real-time and dekadally updated monitoring results of land cover, monitoring of cropland

degradation was carried out according to the UNCCD's framework, which includes 3 subindicators: land cover, land productivity, and soil organic carbon.

Monitoring results of subindicator: Land cover

Based on the land cover transition matrix shown in Table 3, the cropland degradation assessment result for the subindicator of land cover was obtained using the cropland degradation extent of baseline period (2000 to 2015) and target period (2015 to 2022). According to Fig. 7, most of the cropland in the study area maintained a stable state, showing a large continuous distribution. However, there are still some areas with degraded cropland, such as the peri-urban area, the arid northwest area, and the mountainous southwest area, showing a scattered distribution. Meanwhile, a large amount of improved cropland can be found in the study area, also with a sporadic distribution, but with a clear aggregation in the mountainous areas. This is related to the ecological engineering and revegetation land use policy carried out in China since 2000, which led to the cropland with steeper slopes located in mountainous areas was retired to grassland or forest.

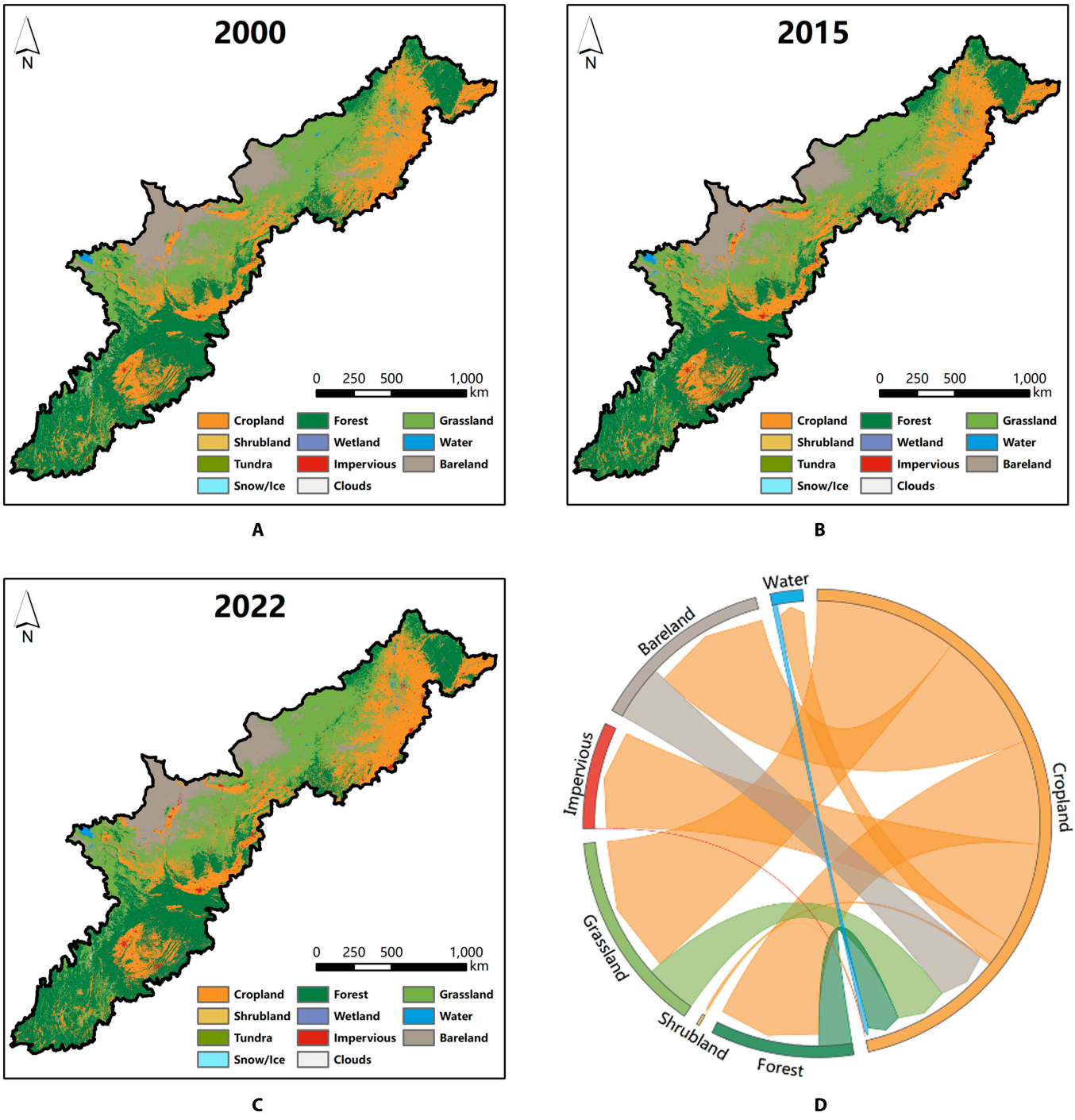

Fig. 4. Annual land cover maps of (A) 2000, (B) 2015, and (C) near real time (2022 August 20). (D) The cropland transfer analysis result of 2000 and near real time.

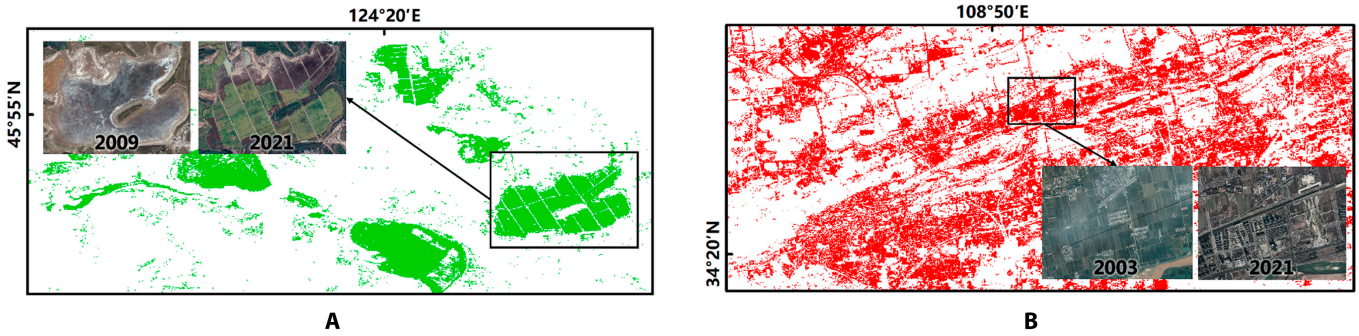

Fig. 5. Detailed cropland dynamics. (A) Cropland expansion in Daqing, Heilongjiang and (B) cropland contraction in Xian, Shaanxi.

Monitoring results of subindicator: Land productivity

The subindicator of land productivity was measured from 3 aspects: *Trend*, *State*, and *Performance* (Fig. 8). Subject to the calculation of the 3 factors, *Trend* and *State* can reflect the degradation and improvement of cropland, while *Performance* can only characterize the degradation. Using the lookup table in Table 4, the final monitoring results of land productivity was obtained. Generally, similar monitoring results for *Trend* and *State* can be observed, which indicates that most cropland in the study area has been more productive in recent years than in the baseline years. For the monitoring results of *Performance*, most cropland in the study area shows not degraded, and the degradation mainly located at the northwest of the middle region of MSBBC, concentrated in peri-urban, mountainous terraces, and desertified areas. It is evident that the productivity of cropland in these areas is lower within the same ecological subzone. Generally, according to the final monitoring results combining *Trend*, *State*, and *Performance*, the productivity of most cropland across the study area is stable or has improved compared to previous years, and degraded cropland is sporadically distributed, with a majority occurring in suburbs.

Monitoring results of subindicator: Soil organic carbon

Taking advantage of IPCC Tier 1 methods [56], the subindicator of soil organic carbon was obtained based on the soil classification map of HWSD and IPCC climate zones (Fig. 9). The majority of the cropland in the study area shows a stable condition according to the results. Nonetheless, there is improvement and degradation in fragmented fields and the edges of contiguous croplands. For northeast region of the study area, degradation and improvement can be observed in the junction with the forest (zoomed area A in Fig. 9). Besides, with similar results to those of land cover and land productivity, fragmented fields located in drought and desertification are prone to be degradation (zoomed area B and C in Fig. 9). Most of the improvement occurs in the hilly gully areas of the Loess Plateau in the middle region of the study area, largely thanks to ecological restoration projects in this region of China over the last 2 decades (zoomed area D and E in Fig. 9). The improvement along the sides of the ridge can be observed. However, degradation can also be found in these terraces, such as the new cultivated cropland in the southwest mountains (zoomed area F in Fig. 9).

Integrated cropland degradation in MSBBC

The final cropland degradation monitoring results were further evaluated using the workflow shown in Fig. 3. The monitoring results show that over 90% of the cropland in the study area is not degraded (Fig. 10A). Cropland degradation has the largest share in the Southeast region, accounting for 9.68% of the region's cropland. The Middle region is the next most degraded with 7.87%, while the Northeast region is the least degraded with 3.36%. To further analyze the spatial distribution characteristics of degraded cropland, we calculated the degradation intensity (i.e., the percentage of degraded cropland) within a 1-km grid and analyzed the spatial aggregation of degradation intensity using spatial analysis algorithms. The calculated global Moran index was 0.24 and passed the 1% significance test, indicating that the degraded cropland had a spatial positive correlation in spatial distribution and showed a strong aggregation. From the degradation intensity shown in Fig. 10B, the degradation of cropland is mainly concentrated in the Horqin sands with serious land desertification in the northeast, the northwestern part of the Loess Plateau with serious soil erosion in the central Shaanxi-Gansu-Ningxia junction, and the mountainous areas with serious soil erosion in northwest and southwest Sichuan, which may be related to the poor agricultural conditions (climate, topography, etc.) in these areas. In addition, to facilitate land policy planning, we calculated the intensity of cropland degradation for each county (Fig. 10C). Overall, the distribution of cropland degradation intensity varies greatly among different counties in the study area. The counties with higher degradation intensity are mainly located west of Huline. Besides, some of the districts and counties located near the city centers also have a higher intensity of cropland degradation, which are scattered throughout the study area.

Open platform for near real-time cropland dynamic monitoring

Our work constructed a framework for the near real-time and dekadally updated cropland monitoring from 3 perspectives: land cover change, conditions, and degradation monitoring. Here, we provide an accessible open platform (https://leyu.users.earthengine.app/view/fgp-cropland) developed based on this framework (Fig. 11). The cropland map in the platform is updated every 10 d using FROM-GLC Plus and the cropland condition monitoring is realized based on the index anomaly method. The cropland degradation monitoring results are rendered and shown in the platform, including final results

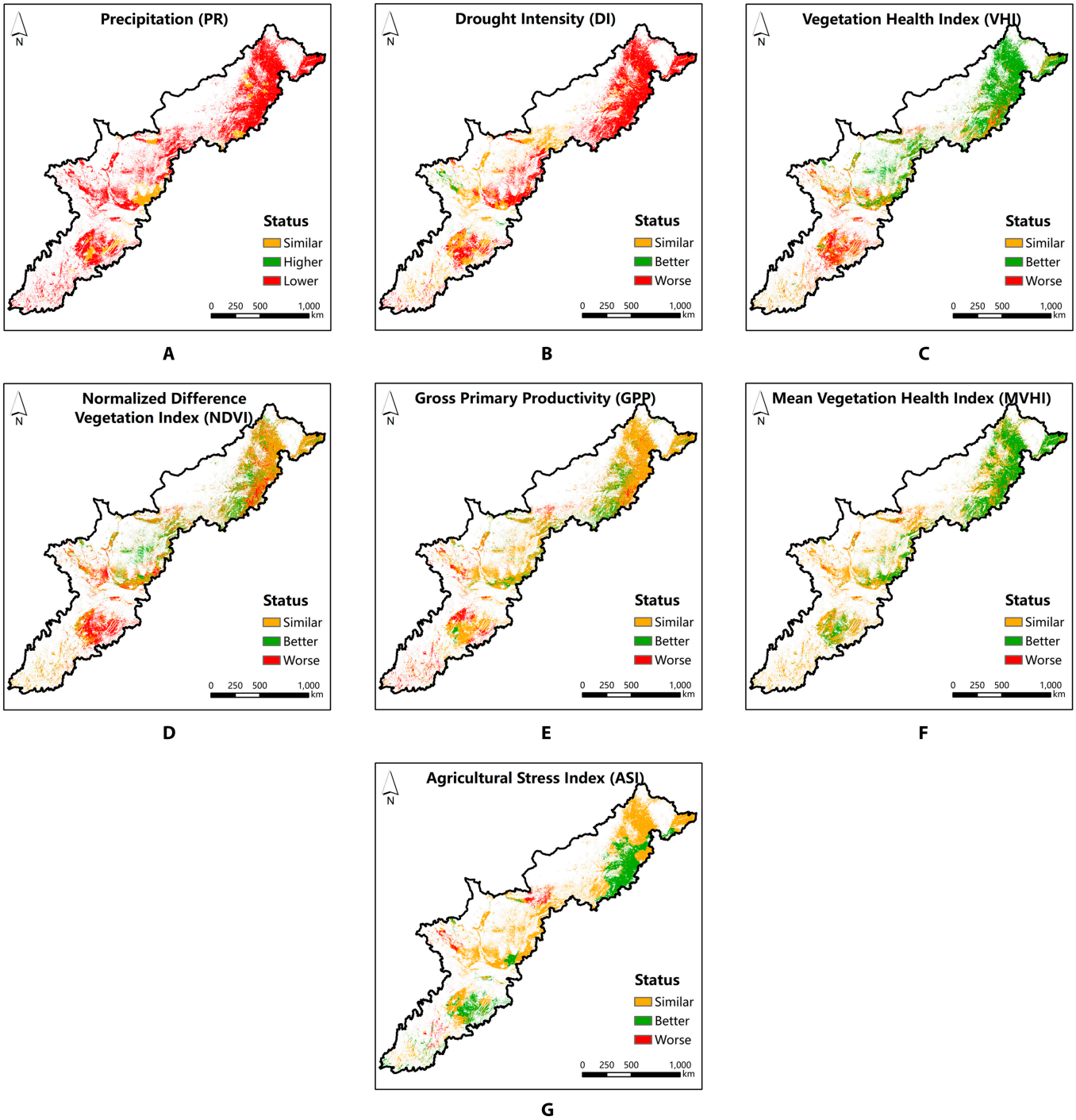

Fig. 6. Cropland condition monitoring results of 2022 August 20, which were developed based on indicators of (A) Precipitation (PR), (B) Drought Intensity (DI), (C) Vegetation Health Index (VHI), (D) Normalized Difference Vegetation Index (NDVI), (E) Gross Primary Productivity (GPP), (F) Mean Vegetation Health Index (MVHI), and (G) Agricultural Stress Index (ASI).

and results of 3 subindicators (i.e., land cover change, land productivity, and soil organic carbon). Specifically, the results can be obtained on both pixel level and county level with the selector in the upper right corner ("Check by County" / "Check by Point"). Users can see cropland condition monitoring results for the point/county of interest on the right by simply clicking on the map on the left.

In addition to the monitoring methods developed in the study area of MSBBC, the open platform can provide the monitoring results of (a) cropland drought, (b) the population exposed to drought, and (c) the degree of drought vulnerability using the guidance of UNCCD [57]. Firstly, the cropland drought was shown using the near real-time cropland map rendered with the drought intensity classes which is obtained using the product of Standardized Precipitation Index [58] and classification method suggested by UNCCD [57]. Secondly, the population exposed to drought is evaluated on the county level based on the drought intensity classification results and population

dataset of WorldPop. With a click on the interested county, users can see the evaluated results on the right. Specifically, the age and sex distribution of the population exposed to drought can also be observed in the bar chart on the right. Thirdly, the degree of drought vulnerability is evaluated using Drought Vulnerability Index (DVI). DVI is recommended to be calculated using 3 components of social, economic, and infrastructural [57]. For these 3 components, UNCCD provides various factors, such as literacy rate, Gross Domestic Product (GDP), safely managed drinking water, etc. However, due to the availability of data, we choose "GDP per capita" for economic to calculate DVI on the county level [59], and the vulnerability is rendered with the county boundary on the left. As more relevant data products are added, the platform estimates of DVI will be further optimized.

Implications and perspectives

According to the degradation monitoring results, we found that cropland degradation of MSBBC showed a significant aggregation in desertified areas (Horqin sands) and mountainous hilly areas (Loess Plateau and west of Sichuan), which implies the possible reasons of degradation, such as topography, precipitation, and cropland management.

In order to obtain the spatial distribution of degraded cropland in relation to topography, we further analyzed the distribution characteristics of degraded and nondegraded cropland

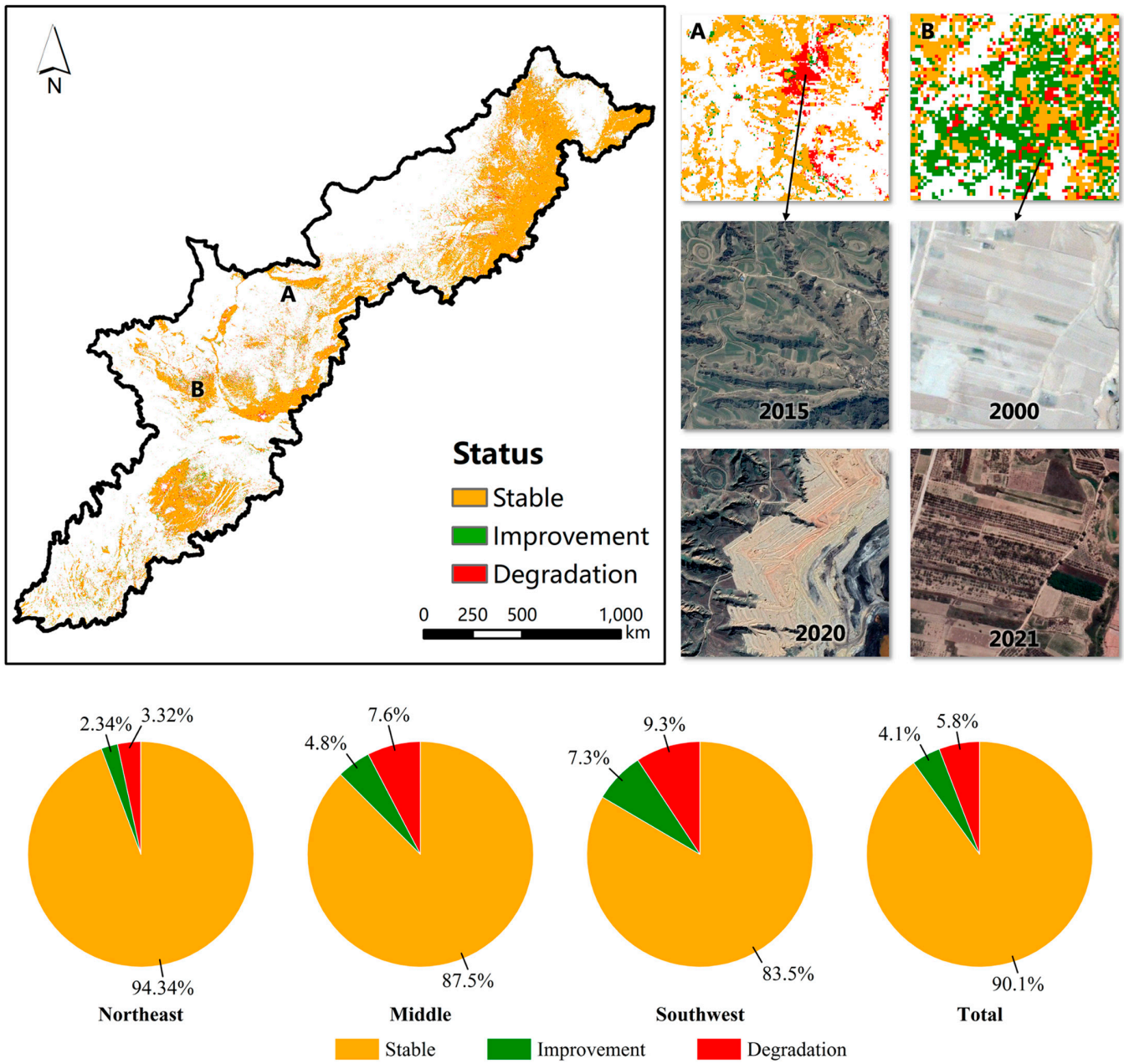

Fig. 7. Cropland degradation monitoring results based on the subindicator of land cover. The zoomed-in areas A and B provide a detailed view of the cropland degradation caused by the shift to bare land and improvement caused by the ecological engineering and revegetation land use policy, respectively.

in terms of 2 key topographic factors, slope and elevation, based on the 30-m Shuttle Radar Topography Mission data. We found that the slope of degraded cropland is steeper and the elevation is higher compared to undegraded cropland. Among the degraded cropland, the percentage of terraces and sloping cropland (slope > 2°) is 52.50%, while the percentage of terraces and sloping cropland of undegraded cropland is 43.29%. The percentage of degraded cropland located at high elevation (>1,500 m) is 20.08%, and the percentage of undegraded cropland located at high elevation is 12.11%. Based on the analysis results shown in Fig. 12A, from the southwest to the northeast, the slope of cropland gradually tended to level off, and the slope of degraded cropland within the sections is higher, which again suggested that cropland at steeper slope may be more prone to degradation.

Insufficient precipitation is another potential factor contributing to the degradation of cropland in MSBBC, as most of the degraded cropland in northeast and middle sections was located in arid or semiarid area of China (i.e., the west of the 400 mm/y precipitation isoline). This pattern was further proved using the results of superimposed analysis with precipitation product of GSMaP. The statistical results shown in

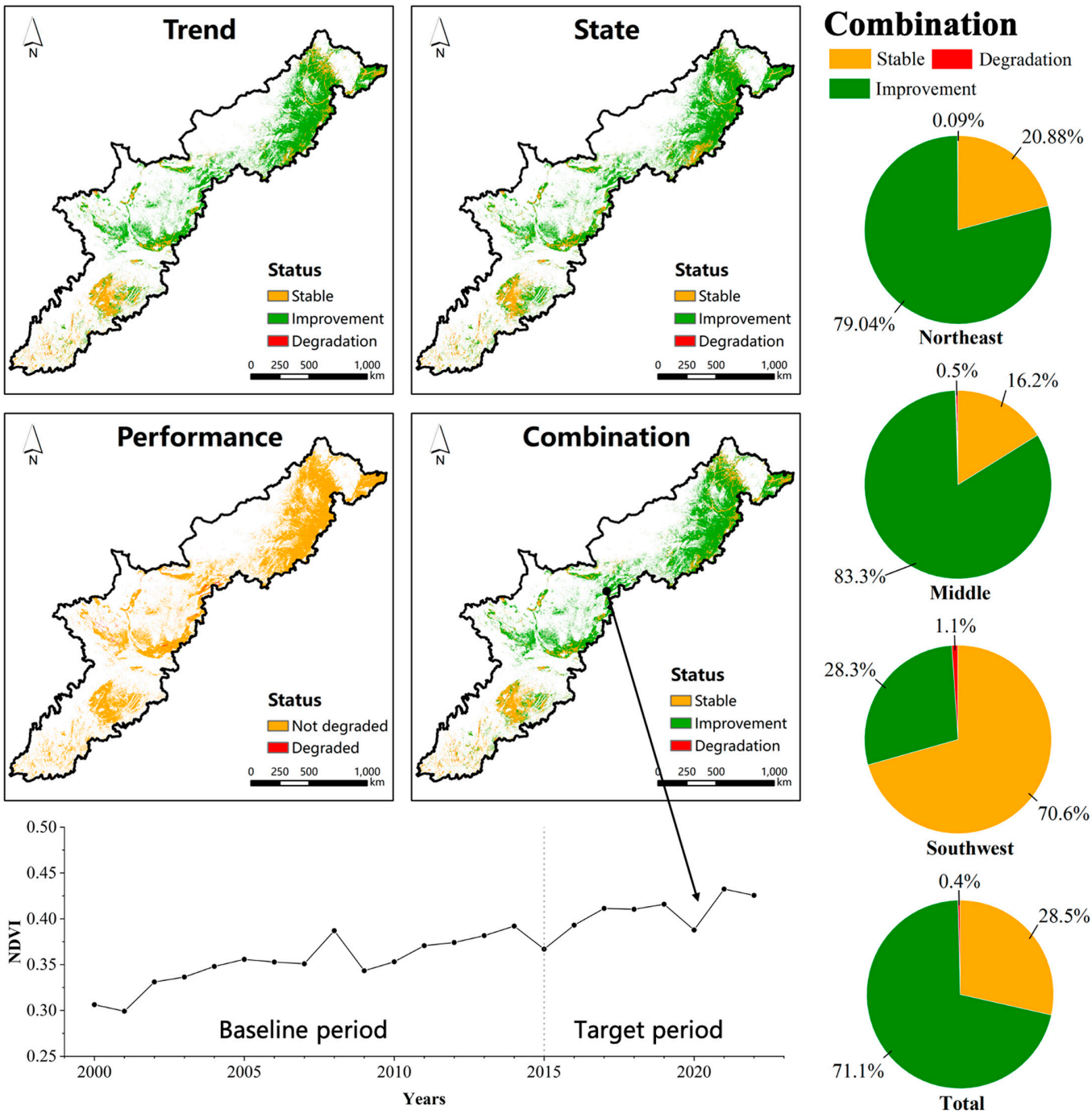

Fig. 8. Cropland degradation monitoring results based on the subindicator of land productivity. The line graph depicts a steady increase in the NDVI since 2000 and notably higher NDVI values for target period, showing improved land productivity.

Fig. 12B suggested that degraded cropland tended to have less precipitation. However, this difference is not apparent with the degradation in southwest section of MSBBC, which indicated that the degradation may be induced by the shortage of irrigation measures for the cropland in mountainous areas.

Meanwhile, the degradation of cropland may be further accelerated by inappropriate cropland use. In the past decades, increasing population and rapid economic development have aggravated the conflict between humans and land in China. This contradiction is further exacerbated by the chronic water shortage, land desertification, and soil erosion in MSBBS, resulting in overcultivation. It has been reported that intensive cropland use in this region, including successive crop and neglect of fallow and crop rotation, has led to degradation over the past half-century [60–62]. Furthermore, cropland degradation has been exacerbated by further soil nutrient loss due to land desertification in the northeast section and soil erosion problems on the central Loess Plateau and mountainous regions in the southwest section.

Additionally, for possible future change in MSBBS, simulated results from CMIP6 under 4 radiative forcing scenarios (SSP1-2.6, SSP2-4.5, SSP3-7.0, and SSP5-8.5) reveal extraordinary increase in NPP and precipitation in MSBBC in the coming decades [63]. It indicates a great production potential for cropland under the influence of future nature conditions. For the max exploitation of this potential, measures should be taken for sustainable cropland use in MSBBC to curb the further cropland degradation. Counties with high degradation intensity (as shown in Fig. 10C) should pay more attention on the cropland restoration. Conservation tillage, such as stubble,

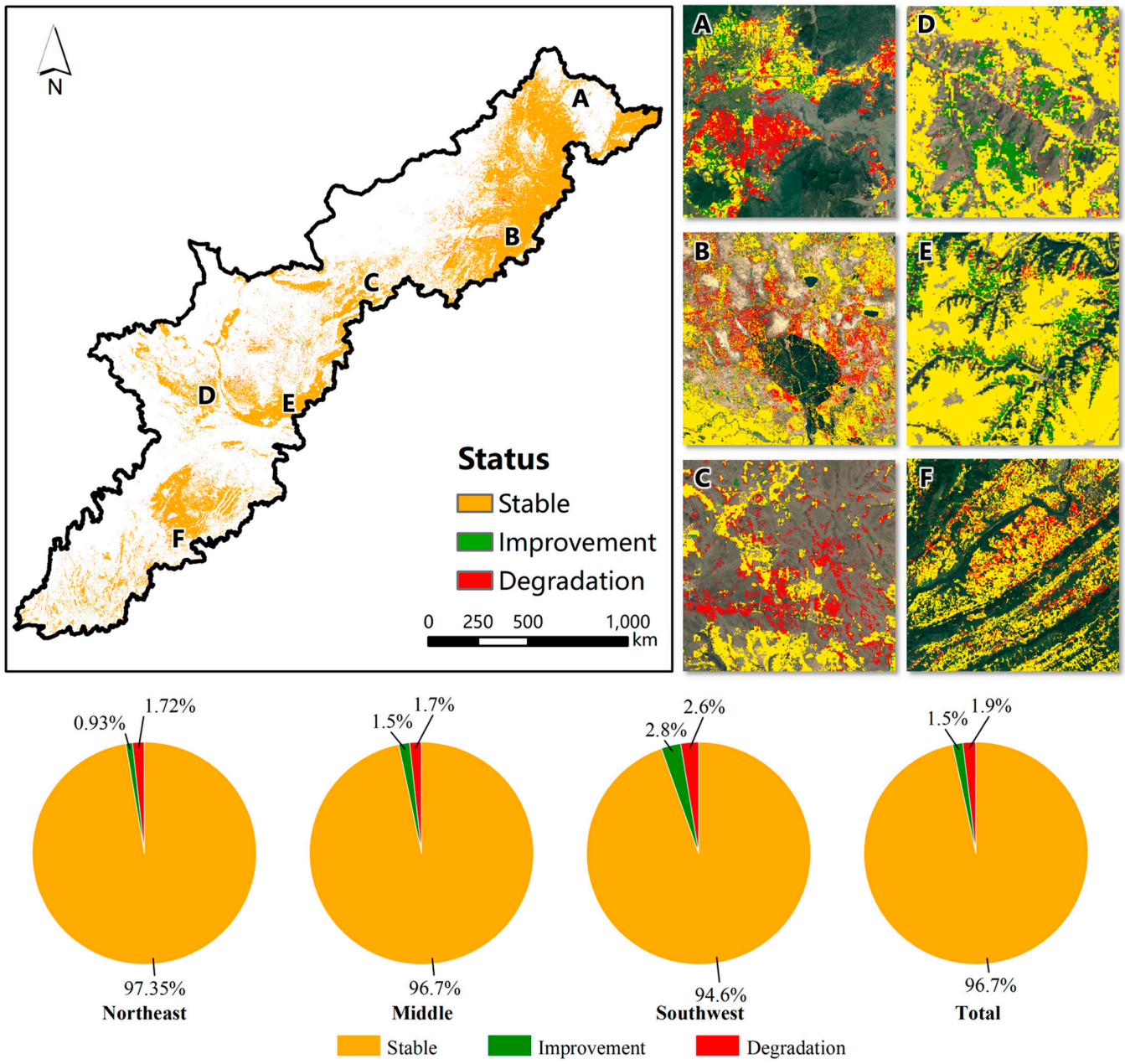

Fig. 9. Cropland degradation monitoring results based on the subindicator of soil organic carbon. The zoomed-in results on the right are superimposed on the Google Earth images.

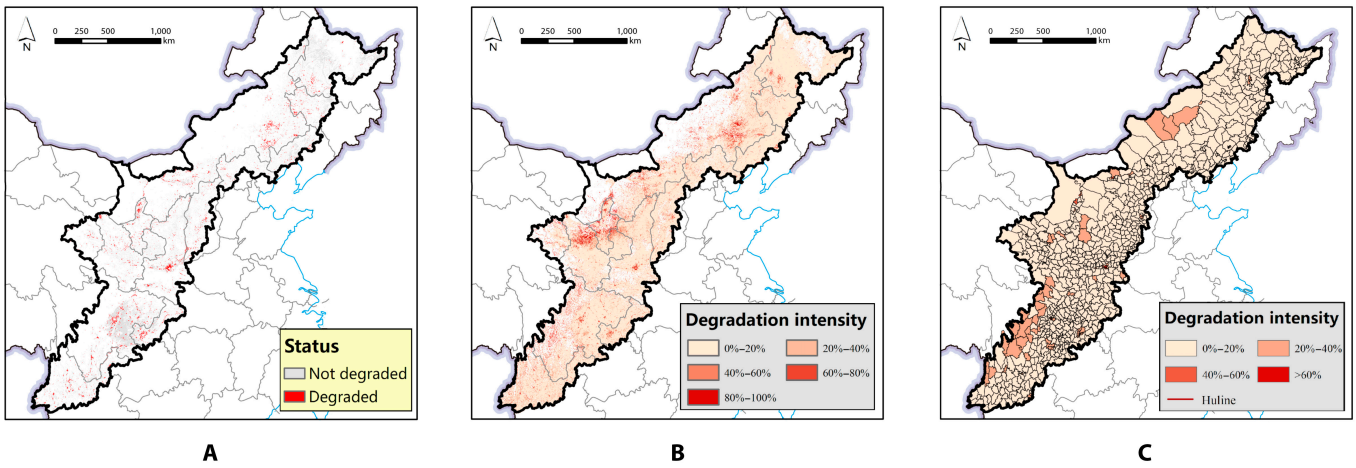

Fig. 10. Final cropland degradation monitoring results. (A) Thirty-meter monitoring result. (B) Degradation intensity in 1-km grids. (C) Degradation intensity in county level.

fallow, and nontillage, is a potentially useful practice for the rest and recuperation of cropland. Additionally, for southern double or tribble maturity zones, improved tillage systems also contribute to the soil nutrient accumulation and recovery. For example, seasonal fallow, including "winter break–summer planting" and one less season of rice planting, can help relieve the tension and fatigue of cropland. Cropland ecological projects is another measure to curb the degradation. Site-specific soil improvement and land reclamation, such as soil structure improvement, construction of irrigation facilities and terrace transformation, is necessary to provide proper conditions for cultivation. In areas where wind, sand, frost, and other disasters are serious, reasonable planning of field protection forest system construction should be considered as an effective measure for improving agricultural production conditions.

Uncertainties and limitations

In this study, we developed an operational assessment framework for near real-time cropland dynamic monitoring. By linking FROM-GLC Plus and FAO ASIS, our framework can provide near real-time and dekadally updated cropland extent, cropland condition, and cropland degradation monitoring results. Additionally, an open platform of its application is provided, which further indicates the near real-time monitoring capability of our framework for cropland at pixel and county scales.

However, there are still some uncertainties and limitations should be figured out for potential future applications. Due to the limitation of computational efficiency, our framework needs to rely on some publicly available datasets of GEE, which means that it is not possible to unify all the data to 30-m resolution, resulting in some monitoring results with plaque problems. In addition, thanks to FROM-GLC Plus, the land cover classification results are updated in near real time dekadally, but the difference in temporal resolution of different data products causes some monitoring results to be out of synchronization. Another issue arising from the computational efficiency is that the open platform developed in this paper is still difficult to scale up, as classification, monitoring, and statistics would take longer, making it difficult to guarantee the near real-time nature of the platform. Another limitation of our framework is that the mapping and monitoring results still relies on manual update. In the future, if there is automatic result push that relies

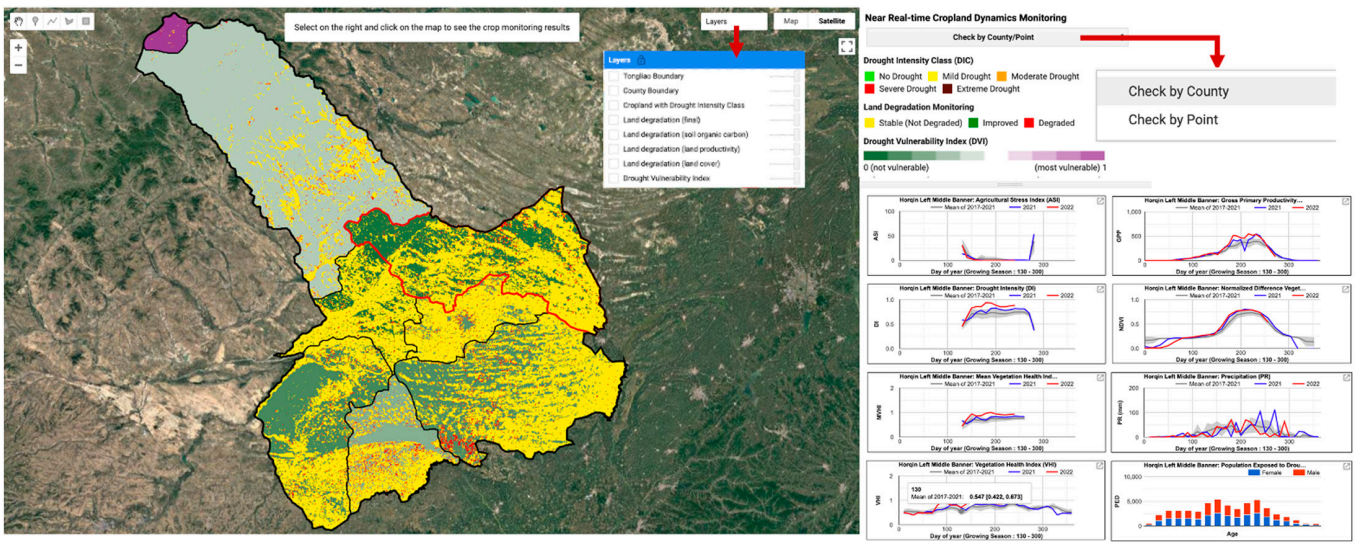

Fig. 11. Open platform for near real-time cropland dynamics monitoring (https://leyu.users.earthengine.app/view/fgp-cropland).

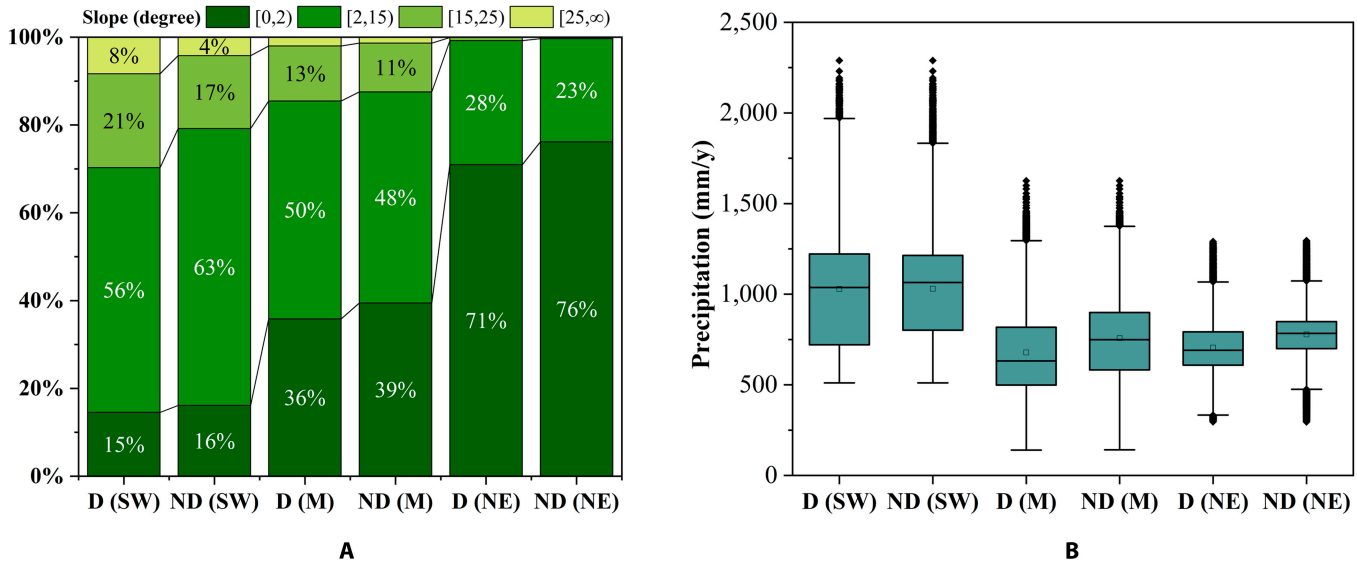

Fig.12. Analysis of slope and precipitation on degraded and undegraded cropland. (A) Percentage of degraded and undegraded cropland with different slope intervals. (B) Distribution of annual precipitation among degraded and undegraded cropland. D, degraded; ND, not degraded; SW, southwest section; M, middle section; NE, northeast section.

on source data (such as Landsat imagery) update, it will further improve the real time and usability of the workflow.

Conclusion

Cropland mapping and monitoring has always been an important application of remote sensing. Despite the wide variety of methods employed in this field, there is still a lack of an integrated and near real-time framework or platform for cropland dynamic monitoring, which makes it difficult to provide operational assessment tool for agricultural production and management. In this paper, taking advantage of FROM-GLC Plus, FAO ASIS, and the monitoring method suggested by UNCCD, we developed a near real-time monitoring framework for cropland extent change, crop conditions, and cropland degradation in the study area of MSBBC. We found that China's ecological restoration projects made remarkable achievement, and degradation in MSBBC showed a substantial aggregation pattern, particularly entangled with topography, precipitation, and way of cropland use, which suggested that measures such as conservation tillage, improved tillage systems, and cropland ecological projects should be implemented to achieve sustainable cropland use. Our framework can provide convenient access to high-spatiotemporal-resolution cropland maps (30 m, dekadal) and instant (near real time) cropland monitoring results, especially with the open platform presented here. Thus, our work improves the real time of current remote sensing applications and cropland monitoring, which can provide more timely database and technical support for cropland change monitoring, crop health early warning, sustainable development research and decision making.

Acknowledgments

Funding: This work was supported by the National Key R&D Program of China (2019YFA0606601), the Tsinghua University Initiative Scientific Research Program (20223080017), and the National Natural Science Foundation of China (42201367).
Author contributions: L.Y. conceived the experiment, Z.D. conducted the experiment, and all authors analyzed the results and reviewed the manuscript. **Competing interests:** The authors declare that they have no competing interests.

Data Availability

The data supporting the findings of this study are available from the corresponding author upon reasonable request.

References

1. Brown LR. World population growth, soil erosion, and food security. *Science*. 1981;214(4524):995–1002.
2. Bodirsky BL, Popp A, Lotze-Campen H, Dietrich JP, Rolinski S, Weindl I, Schmitz C, Müller C, Bonsch M, Humpenöder F, et al. Reactive nitrogen requirements to feed the world in 2050 and potential to mitigate nitrogen pollution. *Nat Commun*. 2014;5(1):3858.
3. Foley JA, Ramankutty N, Brauman KA, Cassidy ES, Gerber JS, Johnston M, Mueller ND, O'Connell C, Ray DK, West PC, et al. Solutions for a cultivated planet. *Nature*. 2011;478(7369):337–342.
4. Baumann M, Kuemmerle T, Elbakidze M, Ozdogan M, Radeloff VC, Keuler NS, Prishchepov AV, Kruhlov I, Hostert P. Patterns and drivers of post-socialist farmland abandonment in Western Ukraine. *Land Use Policy*. 2011;28(3):552–562.
5. Wang J, Chen YQ, Shao XM, Zhang YY, Cao YG. Land-use changes and policy dimension driving forces in China: Present, trend and future. *Land Use Policy*. 2012;29(4):737–749.
6. Meyfroidt P, Schierhorn F, Prishchepov AV, Müller D, Kuemmerle T. Drivers, constraints and trade-offs associated with recultivating abandoned cropland in Russia Ukraine and Kazakhstan. *Global Environ Change*. 2016;37:1–15.
7. Du ZR, Yang JY, Ou C, Zhang T. Agricultural land abandonment and retirement mapping in the northern China crop-pasture band using temporal consistency check and trajectory-based change detection approach. *IEEE Trans Geosci Remote Sens*. 2022;60:1–12.

8. Gao F, Zhang XY. Mapping crop phenology in near real-time using satellite remote sensing: Challenges and opportunities. *J Remote Sens*. 2021;2021:Article 8379391.
9. Mandal D, Kumar V, Ratha D, Dey S, Bhattacharya A, Lopez-Sanchez JM, McNairn H, Rao YS. Dual polarimetric radar vegetation index for crop growth monitoring using sentinel-1 SAR data. *Remote Sens Environ*. 2020;247: Article 111954.
10. Weiss M, Jacob F, Duveiller G. Remote sensing for agricultural applications: A meta-review. *Remote Sens Environ*. 2020;236:Article 111402.
11. Thenkabail PS, Hanjra MA, Dheeravath V, Gumma M. A holistic view of global croplands and their water use for ensuring global food security in the 21st century through advanced remote sensing and non-remote sensing approaches. *Remote Sens*. 2010;2(1):211–261.
12. Thenkabail PS, Knox JW, Ozdogan M, Gumma MK, Congalton RG, Wu ZT, Milesi C, Finkral A, Marshall M, Mariotto I, et al. Assessing future risks to agricultural productivity, water resources and food security: How can remote sensing help? *Photogram Eng Remote Sen*. 2012;78(8):773–782.
13. Gong P. China needs no foreign help to feed itself. *Nature*. 2011;474(7349):7–7.
14. Yu L, Wang J, Clinton N, Xin QC, Zhong LH, Chen YL, Gong P. FROM-GC: 30 m global cropland extent derived through multisource data integration. *Intl J Digital Earth*. 2013;6(6):521–533.
15. Liu LY, Zhang X, Gao Y, Chen XD, Shuai X, Mi J. Finer-resolution mapping of global land cover: Recent developments, consistency analysis, and prospects. *J Remote Sens*. 2021;2021:Article 5289697.
16. Liu LY, Wang JH, Bao YS, Huang WJ, Ma ZH, Zhao CJ. Predicting winter wheat condition, grain yield and protein content using multi-temporal EnviSat-ASAR and Landsat TM satellite images. *Int J Remote Sens*. 2006;27(4):737–753.
17. Huang D, Wang K, Wu WL. Problems and strategies for sustainable development of farming and animal husbandry in the agro-pastoral transition zone in northern China (APTZNC). *Int J Sustain Dev World Ecol*. 2007;14(4):391–399.
18. Wang XY, Guo HD, Luo L, Chang RC. From Hu Huanyong line to mid-Spine Belt of beautiful China: Breakthrough in scientific cognition and change in development mode. *Bull Chin Acad Sci*. 2021;36(9):1058–1065.
19. Guo HD, Wang XY, Wu BF, Li XW. Cognizing population density Demarcative line (Hu Huanyong-line) based on space technology. *Bull Chin Acad Sci*. 2016;31(12):1385–1394.
20. Yang YJ, Wang K, Liu D, Zhao X, Fan J. Effects of land-use conversions on the ecosystem services in the agro-pastoral ecotone of northern China. *J Clean Prod*. 2020;249: Article 119360.
21. Yao YF, Ge NN, Yu S, Wei XR, Wang X, Jin J, Liu X, Shao M, Wei Y, Kang L. Response of aggregate associated organic carbon, nitrogen and phosphorous to re-vegetation in agro-pastoral ecotone of northern China. *Geoderma*. 2019;341:172–180.
22. Wang YS, Li YH. Promotion of degraded land consolidation to rural poverty alleviation in the agro-pastoral transition zone of northern China. *Land Use Policy*. 2019;88:Article 104114.
23. Becker-Reshef I, Justice C, Sullivan M, Vermote E, Tucker C, Anyamba A, Small J, Pak E, Masuoka E, Schmaltz J, et al. Monitoring global croplands with coarse resolution earth observations: The global agriculture monitoring (GLAM) project. *Remote Sens*. 2010;2(6):1589–1609.
24. Wu BF, Meng JH, Li QZ, Yan NN, Du X, Zhang M. Remote sensing-based global crop monitoring: Experiences with China's CropWatch system. *Intl J Digital Earth*. 2014;7(2):113–137.
25. Joint Research Center (JRC). Monitoring Agricultural ResourceS (MARS) [Internet]. 2015. [accessed 29 Oct 2022] http://mars.jrc.ec.europa.eu/
26. United States Agency for International Development (USAID). Famine Early Warning Systems Network (FEWS NET) [Internet]. 2021. [accessed 29 Oct 2022] http://www.fews.net/Pages/default.aspx
27. Food and Agriculture Organization of the United Nations (FAO). Global Information and Early Warning System (GIEWS) [Internet]. [accessed 29 Oct 2022] https://www.fao.org/giews
28. Food and Agriculture Organization of the United Nations (FAO). AgroMaps [Internet]. [accessed 29 Oct 2022] https://gaez.fao.org/pages/agromaps
29. United States Department of Agriculture (USDA). Crop Explorer [Internet]. [accessed 30 Oct 2022] https://ipad.fas.usda.gov/cropexplorer/
30. Whitcraft AK, Becker-Reshef I, Justice CO, Gifford L, Kavvada A, Jarvis I. No pixel left behind: Toward integrating earth observations for agriculture into the United Nations sustainable development goals framework. *Remote Sens Environ*. 2019;235:Article 111470.
31. Eberhardt IDR, Schultz B, Rizzi R, Sanches ID, Formaggio AR, Atzberger C, Mello MP, Immitzer M, Trabaquini K, Foschiera W, et al. Cloud cover assessment for operational crop monitoring Systems in Tropical Areas. *Remote Sens*. 2016;8(3):Article 219.
32. Gumma MK, Thenkabail PS, Teluguntla PG, Oliphant A, Xiong J, Giri C, Pyla V, Dixit S, Whitbread AM. Agricultural cropland extent and areas of South Asia derived using Landsat satellite 30-m time-series big-data using random forest machine learning algorithms on the Google earth engine cloud. *GIScience Remote Sens*. 2020;57(3):302–322.
33. Thenkabail PS, Biradar CM, Noojipady P, Dheeravath V, Li Y, Velpuri M, Gumma M, Gangalakunta ORP, Turral H, Cai X, et al. Global irrigated area map (GIAM), derived from remote sensing, for the end of the last millennium. *Int J Remote Sens*. 2009;30(14):3679–3733.
34. Yu L, Du ZR, Dong RM, Zheng J, Tu Y, Chen X, Hao P, Zhong B, Peng D, Zhao J, et al. FROM-GLC plus: Toward near real-time and multi-resolution land cover mapping. *GIScience Remote Sens*. 2022;59(1):1026–1047.
35. Shen RQ, Dong J, Yuan WP, Han W, Ye T, Zhao WZ. A 30 m resolution distribution map of maize for China based on Landsat and sentinel images. *Int J Remote Sens*. 2022;2022:Article 9846712.
36. Brown CF, Brumby SP, Guzder-Williams B, Birch T, Hyde SB,Mazzariello J, Czerwinski W, Pasquarella VJ, Haertel R, Ilyushchenko S, et al. Dynamic world, near real-time global 10 m land use land cover mapping. *Sci Data*. 2022;9(1):Article 251.
37. Gong P, Wang J, Yu L, Zhao Y, Zhao Y, Liang L, Niu Z, Huang X, Fu H, Liu S, et al. Finer resolution observation and monitoring of global land cover: First mapping results with Landsat TM and ETM+ data. *Int J Remote Sens*. 2013;34(7):2607–2654.
38. Gorelick N, Hancher M, Dixon M, Ilyushchenko S, Thau D, Moore R. Google earth engine: Planetary-scale geospatial analysis for everyone. *Remote Sens Environ*. 2017;202:18–27.

39. Food and Agriculture Organization of the United Nations (FAO). FAO ASIS [Internet]. [accessed 29 Oct 2022] https://www.fao.org/giews/earthobservation/index.jsp?lang=en
40. Symeonakis E, Drake N. Monitoring desertification and land degradation over sub-Saharan Africa. *Int J Remote Sens*. 2004;25(3):573–592.
41. Wessels KJ, Prince SD, Frost PE, van Zyl D. Assessing the effects of human-induced land degradation in the former homelands of northern South Africa with a 1 km AVHRR NDVI time-series. *Remote Sens Environ*. 2004;91(1):47–67.
42. Desa UN. Transforming our world: The 2030 agenda for sustainable development; 2016.
43. Zhao L, Jia K, Liu X, Li J, Xia M. Assessment of land degradation in Inner Mongolia between 2000 and 2020 based on remote sensing data. *Geograp Sust*. 2023;4(2):100–111.
44. Reith J, Ghazaryan G, Muthoni F, Dubovyk O. Assessment of land degradation in semiarid Tanzania—Using multiscale remote sensing datasets to support sustainable development goal 15.3. *Remote Sens*. 2021;13(9):Article 1754.
45. Giuliani G, Mazzetti P, Santoro M, Nativi S, Van Bemmelen J, Colangeli G, Lehmann A. Knowledge generation using satellite earth observations to support sustainable development goals (SDG): A use case on land degradation. *Int J Appl Earth Obs Geoinf*. 2020;88:Article 102068.
46. Sims NC, Green C, Newnham GJ, England JR, Held A, Wulder MA, Herold M, Cox SJD, Huete AR, Kumar L. Good practice guidance. SDG indicator 15.3. 1: proportion of land that is degraded over total land area. United Nations Convention to Combat Desertification (UNCCD); Bonn, Germany; 2017.
47. Sims NC, Newnham GJ, England JR, Guerschman J, Cox SJD, Roxburgh SH, Viscarra Rossel RA, Fritz SWI, Wheeler I. Good Practice Guidance, SDG Indicator 15.3. 1, Proportion of Land That Is Degraded Over Total Land Area. Version 2.0; Bonn, Germany; 2021.
48. Hu HY. The distribution of China's population: With statistical tables and density maps. *Acta Geograph Sin*. 1935;2:33–72.
49. Keith DA, Ferrer-Paris JR, Nicholson E, Bishop MJ, Polidoro BA, Ramirez-Llodra E, Tozer MG, Nel JL, Mac Nally R, Gregr EJ, et al. A function-based typology for Earth's ecosystems. *Nature*. 2022;610(7932):513–518.
50. Wuyun DJ, Sun L, Chen ZX, Hou AH, Crusiol LGT, Yu L, Chen R, Sun Z. The spatiotemporal change of cropland and its impact on vegetation dynamics in the farming-pastoral ecotone of northern China. *Sci Total Environ*. 2022;805:Article 150286.
51. Li SJ, Sun ZG, Tan MH, Guo LL, Zhang XB. Changing patterns in farming–pastoral ecotones in China between 1990 and 2010. *Ecol Indic*. 2018;89:110–117.
52. Jian YQ, Liu ZJ, Gong JZ. Response of landscape dynamics to socio-economic development and biophysical setting across the farming-pastoral ecotone of northern China and its implications for regional sustainable land management. *Land Use Policy*. 2022;122:Article 106354.
53. Kubota T, Shige S, Hashizume H, Aonashi K, Takahashi N, Seto S, Hirose M, Takayabu YN, Ushio T, Nakagawa K, et al. Global precipitation map using satellite-borne microwave radiometers by the GSMaP project: Production and validation. *IEEE Trans Geosci Remote Sens*. 2007;45(7):2259–2275.
54. Nachtergaele F, van Velthuizen H, Verelst L, Batjes NH, Dijkshoorn K, van Engelen VWP, Fischer G, Jones A, Montanarela L. The harmonized world soil database. Paper presented at: Proceedings of the 19th World Congress of Soil Science, Soil Solutions for a Changing World; 2010 Aug 1–6; Brisbane, Australia.
55. Dinerstein E, Olson D, Joshi A, Vynne C, Burgess ND, Wikramanayake E, Hahn N, Palminteri S, Hedao P, Noss R, et al. An ecoregion-based approach to protecting half the terrestrial realm. *Bioscience*. 2017;67(6):534–545.
56. Eggleston HS, Buendia L, Miwa K, Ngara T, Tanabe K. 2006 IPCC guidelines for national greenhouse gas inventories; 2006.
57. Barker LJ, Rickards NJ, Sarkar S, Hannaford J, King-Okumu C, Rees G. *Good practice guidance for national reporting on UNCCD strategic objective 3*: To mitigate, adapt to, and manage the effects of drought in order to enhance resilience of vulnerable populations and ecosystems. In United Nations Convention to Combat. 2021.
58. Vose RS, Applequist S, Squires M, Durre I, Menne MJ, Williams CN, Arndt D. NOAA's gridded climate divisional dataset (CLIMDIV). NOAA National Climatic Data Center; 2014.
59. Chen J, Gao M, Cheng S, Hou W, Song M, Liu X, Liu Y. Global 1 km × 1 km gridded revised real gross domestic product and electricity consumption during 1992–2019 based on calibrated nighttime light data. *Sci Data*. 2022;9(1):Article 202.
60. Yang XM, Chen H, Gong YS, Zheng XH, Fan MS, Kuzyakov Y. Nitrous oxide emissions from an agro-pastoral ecotone of northern China depending on land uses. *Agric Ecosyst Environ*. 2015;213:241–251.
61. Chen X, Jiang L, Zhang GL, Meng LJ, Pan ZH, Lun F, An PL. Green-depressing cropping system: A referential land use practice for fallow to ensure a harmonious human-land relationship in the farming-pastoral ecotone of northern China. *Land Use Policy*. 2021;100:Article 104917.
62. Wang ZH, Yao WY, Tang QH, Liu LY, Xiao P, Kong XB, Zhang P, Shi FX, Wang YJ. Continuous change detection of Forest/grassland and cropland in the loess plateau of China using all available Landsat data. *Remote Sens*. 2018;10(11):Article 1775.
63. Zheng S, Pan Y, Yu L, Liu S, Peng D. Possible future movement of the Hu line based on IPCC CMIP6 scenarios. *Environ Res Commun*. 2022;4(9):Article 095008.